Chemistry – A European Journal

ChemEurJ Chemistry Europe European Chemical Societies Publishing

RESEARCH ARTICLE

Perfect in-Plane [5555] Metallo-Annulene Frameworks and Nonmetallo-Annulene Complexes: A Theoretical Prediction

Qin-Wei Zhang | Qiang Chen | Xiao-Ni Zhao | Rui Wei | Si-Dian Li

Institute of Molecular Science, Shanxi University, Taiyuan, China

Correspondence: Qiang Chen (chenqiang@sxu.edu.cn) | Si-Dian Li (lisidian@sxu.edu.cn)

Received: 20 January 2026 | **Revised:** 5 March 2026 | **Accepted:** 11 June 2026

Keywords: Aromaticity | First principles theory | In-plane [5555] nonmetallo-annulene | In-plane [5555] metallo-annulene | Structures and bonding

ABSTRACT

Inspired by the newly discovered in-plane [55555] metallo-annulene frameworks in 3D $[Os]C_{15}H_{10}$ ([Os] = OsL^1L^2 and L represents PPh_3, CO, or PEt_3 σ-ligands in axial direction) and recently proposed perfect 2D in-plane [55555] metallo-annulene complexes D_{5h} $MC_{15}H_{10}$ (M = Pt, Pd, Ni), based on extensive first-principles theory calculations, we predict herein a series of perfect in-plane [5555] metallo-annulene frameworks in 3D D_{4h} $[Fe]C_{12}H_8$ (**1**, [Fe] = $Fe(CO)_2$) and D_{4h} $[Co]C_{12}H_8^+$ (**2**, [Co] = $Co(CO)_2$) and perfect 2D in-plane [5555] nonmetallo-annulene complexes including D_{4h} $PC_{12}H_8^-$ (**3**), D_{4h} $SC_{12}H_8$ (**4**), and D_{4h} $ClC_{12}H_8^+$ (**5**). Detailed bonding pattern and ring current analyses indicate that planar tetracoordinate metal or nonmetal centers participate in the delocalized π-bonding systems of the annulene complexes, rendering π-aromaticity and extra stability to the systems. Such species with a planar $[12]C_{12}H_8$ annulene ligand can be enlarged in 2D to form the C_{4v} $[Fe]C_{36}H_{16}$ (**6**), D_{4h} $[Co]C_{36}H_{16}^+$ (**7**), D_{4h} $PC_{36}H_{16}^-$ (**8**), D_{4h} $SC_{36}H_{16}$ (**9**), and C_s $ClC_{36}H_{16}^+$ (**10**) and expanded in 3D to generate the tubular nanobelt C_{2v} $(SC_{12}H_4)_{12}$ (**11**) via partial dehydrogenations. The NMR, IR, and UV-vis spectra of the most concerned species **1–5** are computationally simulated to facilitate their future experimental characterizations.

1 | Introduction

Annulenes are defined as a class of closed-ring conjugated compounds with alternating single and double bonds by the International Union of Pure and Applied Chemistry [1–4]. The effective delocalization of π-electrons within the cyclic framework confers unique chemical properties to the systems. Representative annulenes include cyclobutadiene, benzene, and cyclooctatetraene, etc. Annulenes and their ionic derivatives can be used as effective ligands to sandwich various transition metals to form typical out-of-plane metallo-annulene complexes. Ferrocene $[Fe(\eta^5\text{-}C_5H_5)_2]$, synthesized for the first time in the 1950s, has served as a representative metallo-annulene complex in this field, with its research scope stretching into catalysis, biomedicine, materials science, and other multidisciplinary areas, thereby establishing a fundamental foundation for modern organometallic chemistry [5, 6]. Bis(η^6-benzene) chromium $[Cr(\eta^6\text{-}C_6H_6)_2]$ as another prototypical metallo-annulene complex has evolved into a fundamental building block for the design and synthesis of functional nanomaterials, consistently driving advancements in cutting-edge fields such as catalysis and nanotechnology [7, 8]. Furthermore, the scope of metallo-annulene complexes has been extended to actinide, as exemplified by the successful synthesis of bis(cyclooctatetraenyl) uranium (Uranocene) [9]. In addition to classical sandwich architectures, structural motifs such as half-sandwich complexes, helicene complexes, and coplanar complexes (e.g., Grignard reagents) have significantly enriched the structural diversity of such compounds and broadened their potential applications [10–14]. In contrast to the well-known traditional out-of-plane metallo-annulenes, real in-plane metallo-annulenes had remained elusive in the literature before 2025, raising an obvious question to answer in the area: Can a metal or

nonmetal atom be embedded within the framework of annulenes or their derivatives to form stable in-plane metallo-/nonmetallo-annulene complexes?

As an important class of azaannulene derivatives, porphyrins and their analogs do form stable in-plane complexes with various metals, thereby providing important references for the study of in-plane annulene chemistry [15–18]. The "Carbolong Chemistry" pioneered by Xia and his group has provided crucial inspiration for the investigation on in-plane metallo-annulene compounds [19–22]. They synthesized and characterized in 2025 the first in-plane [55555] metallo-annulene frameworks in 3D $[Os]C_{15}H_{10}$ ([Os] = OsL^1L^2 and L represents PPh_3, CO, or PEt_3 σ-ligands in the axial direction) [1]. These complexes exhibit a unique bonding pattern, in which the Os atom forms five Os-C σ bonds within the $[15]C_{15}H_{10}$ annulene plane and its d_{xz} and d_{yz} orbitals participate in the π-conjugation with five pentagons in the annulene plane, making the systems fundamentally different from traditional out-of-plane metallo-annulene complexes. Our group subsequently predicted late in 2025 a series of perfect 2D in-plane [55555] metallo-annulene complexes D_{5h} $MC_{15}H_{10}$ (M = Pt, Pd, Ni) at first-principles theory level [2] wherein the planar pentacoordinate metal (ppM) center shared by five equivalent pentagons around it and the $[15]C_{15}H_{10}$ annulene ligand match both geometrically and electronically in a $5\sigma + 2\pi$ coordination bonding pattern, without the two additional axial σ-donor ligands needed to stabilize the systems. The coordination bonding patterns between the ppM center and $[15]C_{15}H_{10}$ annulene ligand in these perfect 2D species prove to resemble that in the experimentally observed 3D $[Os]C_{15}H_{10}$ [1], rendering overall π-aromaticity and extra stability to the systems.

Using a smaller planar $[12]C_{12}H_8$ annulene as ligand and based on extensive first-principles theory calculations and analyses, we predict herein possible existence of the perfect in-plane [5555] metallo-annulene frameworks in 3D D_{4h} $[Fe]C_{12}H_8$ (**1**, [Fe] = $Fe(CO)_2$) and D_{4h} $[Co]C_{12}H_8^+$ (**2**, [Co] = $Co(CO)_2$) and perfect 2D in-plane [5555] nonmetallo-annulene complexes including D_{4h} $PC_{12}H_8^-$ (**3**), D_{4h} $SC_{12}H_8$ (**4**) and D_{4h} $ClC_{12}H_8^+$ (**5**) which contain a planar tetracoordinate metal (ptM) or planar tetracoordinate nonmetal (ptNM) center. The ptM $3d_{xz}$ and $3d_{yz}$ and ptNM $2p_z$ atomic orbitals participate in the delocalized π-bonding systems of the annulene complexes, making the species π-aromatic in nature and highly stable both thermodynamically and dynamically. These complexes can be expanded in 2D to form the C_{4v} $[Fe]C_{36}H_{16}$ (**6**, [Fe] = $Fe(CO)_2$), D_{4h} $[Co]C_{36}H_{16}^+$ (**7**, [Co] = $Co(CO)_2$), D_{4h} $PC_{36}H_{16}^-$ (**8**), D_{4h} $SC_{36}H_{16}$ (**9**), and C_s $ClC_{36}H_{16}^+$ (**10**) and in 3D to generate the tubular nanobelt C_{2v} $(SC_{12}H_4)_{12}$ (**11**) via partial dehydrogenations.

2 | Theoretical Methods

All theoretical calculations in this work were performed using the Gaussian 16 software [23]. Full structural optimizations and frequency analyses were comparatively carried out at both the PBE0 [24] and B3LYP [25] hybrid density functional theory levels, with the 6–311+G(d,p) basis sets [26–28] employed for Fe, Ni, P, S, Cl, C, O, and H atoms and SDD basis sets along with the corresponding effective core potentials [29] utilized for Ru, Os, Rh, and Ir. The PBE0 and B3LYP approaches turned out to agree well with each other and produced practically the same results for the species concerned in this work. Frequency calculations confirmed that all the structures obtained are true local minima on the potential energy surface without imaginary vibrational frequencies. To elucidate the detailed bonding characteristics, adaptive natural density partitioning (AdNDP) analyses were conducted using the Multiwfn software [30–32], and the resulting bonding patterns were visualized using GaussView. To evaluate the dynamic stability of structures **1–5**, Born-Oppenheimer molecular dynamics (BOMD) simulations were performed using the CP2K package [33–35]. Isotropic chemical shielding surface (ICSS) [36, 37], anisotropic current-induced density (ACID) [38, 39], and gauge-including magnetically induced current (GIMIC) analyses [40–42] were performed to validate the π-aromaticity of complexes **1–5**. The results were visualized using specific software programs: ICSS with Multiwfn and VMD, ACID plots with POV-Ray, and GIMIC data with ParaView. The NMR chemical shifts, infrared (IR), Raman, and UV-vis spectra of complexes **1–5** were simulated at the PBE0/6-311+G(d,p) level. For the NMR calculations, the Solvation Model based on Density (SMD) was employed with chloroform as the solvent [47] and tetramethylsilane (TMS) as the chemical shift reference. In addition, energy decomposition analyses with natural orbitals for chemical valence (EDA-NOCV) [48–50] were performed on both D_{4h} $[Fe]C_{12}H_8$ (**1**) and D_{4h} $[Co]C_{12}H_8^+$ (**2**) using the ADF program package [51] at the PBE0/TZ2P level of theory to elucidate their coordination bonding patterns.

3 | Results and Discussions

3.1 | Structures and Stabilities

The optimized structures of the perfect in-plane [5555] metallo-annulene frameworks in singlet D_{4h} $[Fe]C_{12}H_8$ (**1**, $^1A_{1g}$) ([Fe] = $Fe(CO)_2$) and D_{4h} $[Co]C_{12}H_8^+$ (**2**, $^1A_{1g}$) ([Co] = $Co(CO)_2$) and triplet in-plane [5555] nonmetallo-annulene complexes including D_{4h} $PC_{12}H_8^-$ (**3**, $^3A_{1g}$), D_{4h} $SC_{12}H_8$ (**4**, $^3A_{1g}$), and D_{4h} $ClC_{12}H_8^+$ (**5**, $^3A_{1g}$) are depicted in Figure 1 at PBE0 level. The corresponding results at B3LYP are comparatively summarized in Figure S1. Detailed frequency analyses indicate that these metal- or nonmetal-centered [5555] annulene complexes are all true minima on the potential energy surfaces of the systems, with the lowest vibrational frequencies of 15.69, 73.41, 75.26, 88.04, and 108.95 cm^{-1} at PBE0, respectively. The ptM (M = Fe, Co) or ptNM (M = P, S, Cl) atom in these complexes is located exactly at the center of the complexes shared by four equivalent pentagons around it, forming four covalent σ-bonds with four C atoms on the inner ring of the $[12]C_{12}H_8$ annulene with bond lengths between 1.81 and 1.89 Å. The C-C bond lengths range from 1.37 to 1.43 Å, slightly shorter than the theoretical C-C single-bond length of 1.50 Å. The HOMO-LUMO (H-L) gaps of the singlet D_{4h} **1** and D_{4h} **2** are 3.49 eV and 3.52 eV, respectively. For triplet D_{4h} **3**, D_{4h} **4**, and D_{4h} **5**, the α-spin H-L gaps turn out to be 4.10 eV, 4.28 eV, and 3.52 eV, while the corresponding β-spin H-L gaps appear to be 3.36 eV, 2.37 eV, and 3.37 eV, respectively. The large calculated H-L gaps serve strong evidence to support the high chemical stability of these $[12]C_{12}H_8$ annulene complexes.

The dynamic stability of complexes **1–5** was checked by extensive BOMD simulations in 100 ps. As collectively shown in

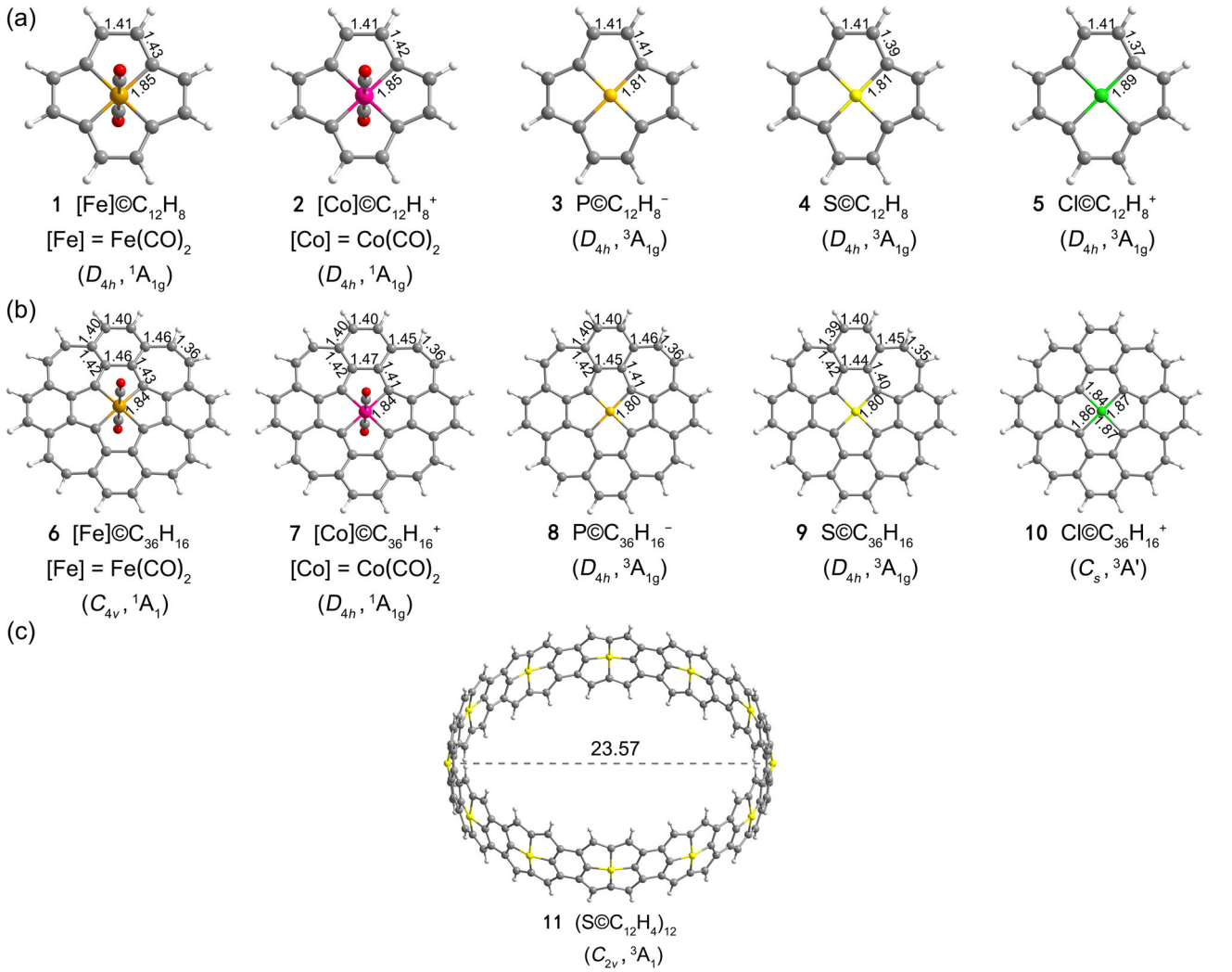

FIGURE 1 | Optimized structures of (a) the perfect in-plane [5555] metallo-annulene frameworks in 3D D_{4h} $[Fe]C_{12}H_8$ (**1**, [Fe] = $Fe(CO)_2$) and D_{4h} $[Co]C_{12}H_8^+$ (**2**, [Co] = $Co(CO)_2$) and perfect 2D in-plane [5555] nonmetallo-annulene complexes D_{4h} $PC_{12}H_8^-$ (**3**), D_{4h} $SC_{12}H_8$ (**4**), and D_{4h} $ClC_{12}H_8^+$ (**5**), (b) in-plane metallo-annulene frameworks in C_{4v} $[Fe]C_{36}H_{16}$ (**6**, [Fe] = $Fe(CO)_2$) and D_{4h} $[Co]C_{36}H_{16}^+$ (**7**, [Co] = $Co(CO)_2$) and in-plane annulene complexes D_{4h} $PC_{36}H_{16}^-$ (**8**), D_{4h} $SC_{36}H_{16}$ (**9**), and C_s $ClC_{36}H_{16}^+$ (**10**), and (c) 3D tubular nanobelt C_{2v} $(SC_{12}H_4)_{12}$ (**11**) at PBE0 level, with the Fe-C, Co-C, P-C, S-C, Cl-C and C-C bond lengths indicated in Å.

Figure 2 that, with the small calculated average root-mean-square deviations of RMSD = 0.05, 0.05, 0.07, 0.07, and 0.06 Å and maximum bond length deviations of MAXD = 0.12, 0.11, 0.18, 0.19, and 0.15 Å for $[Fe]C_{12}H_8$ (**1**) and $[Co]C_{12}H_8^+$ (**2**) at 500 K, $PC_{12}H_8^-$ (**3**) and $SC_{12}H_8$ (**4**) at 1200 K, and $ClC_{12}H_8^+$ (**5**) at 700 K, respectively, these [5555] metallo- and nonmetallo-annulene complexes all appear to be dynamically stable at high temperatures. Although transient fluctuations in RMSD and MAXD values are observed, the deviations are quickly converged to the baselines, with the overall structural integration well maintained in the simulation processes.

The high-symmetry D_{4h} $[Fe]C_{12}H_8$ (**1**) and D_{4h} $[Co]C_{12}H_8^+$ (**2**) can be enlarged in 2D to form the singlet C_{4v} $[Fe]C_{36}H_{16}$ (**6,** [Fe] = $Fe(CO)_2$) with the Fe center slightly off-planed by 0.56 Å and D_{4h} $[Co]C_{36}H_{16}^+$(**7**, [Co] = $Co(CO)_2$) with the Co atom located exactly at the center, with the optimized M-C and C-C bond lengths remained basically unchanged and the H-L gaps decreased to 1.93 eV in **6** and 1.50 eV in **7**, respectively. Similarly, the perfect 2D in-plane [5555] nonmetallo-annulenes D_{4h} $PC_{12}H_8^-$ (**3**), D_{4h} $SC_{12}H_8$ (**4**), and D_{4h} $ClC_{12}H_8^+$ (**5**) can be expanded in 2D to generate the triplet in-plane [5555] nonmetallo-annulenes D_{4h} $PC_{36}H_{16}^-$ (**8**), D_{4h} $SC_{36}H_{16}$ (**9**), and C_s $ClC_{36}H_{16}^+$ (**10**), with the calculated α-spin H-L gaps of 1.66 eV, 1.97 eV, and 2.02 eV and β-spin H-L gaps of 1.40 eV, 1.24 eV, and 1.19 eV, respectively. These enlarged [5555] metallo- and nonmetallo-annulenes with a $[36]C_{36}H_{16}$ annulene ligand all turn out to be true minima of the systems without imaginary vibrational frequencies. More intriguingly, the perfect neutral D_{4h} $SC_{12}H_8$ (**4**) can serve as building blocks to form the slightly distorted 3D tubular nanobelt C_{2v} $(SC_{12}H_4)_{12}$ (**11**) via the partial dehydrogenation reaction [eq. (1)], which results in the first nonmetal-centered annulene nanobelt with an approximate diameter of 23.57 Å reported to date with twelve almost equivalent $SC_{12}H_4$ units, similar to the newly discovered triple stranded porphyrin nanobelts [52]. 1D nanotubes, 2D nanosheets, and 3D nanocrystals composed of periodically distributed $PtMC_{12}$ or $PtNMC_{12}$ building blocks could

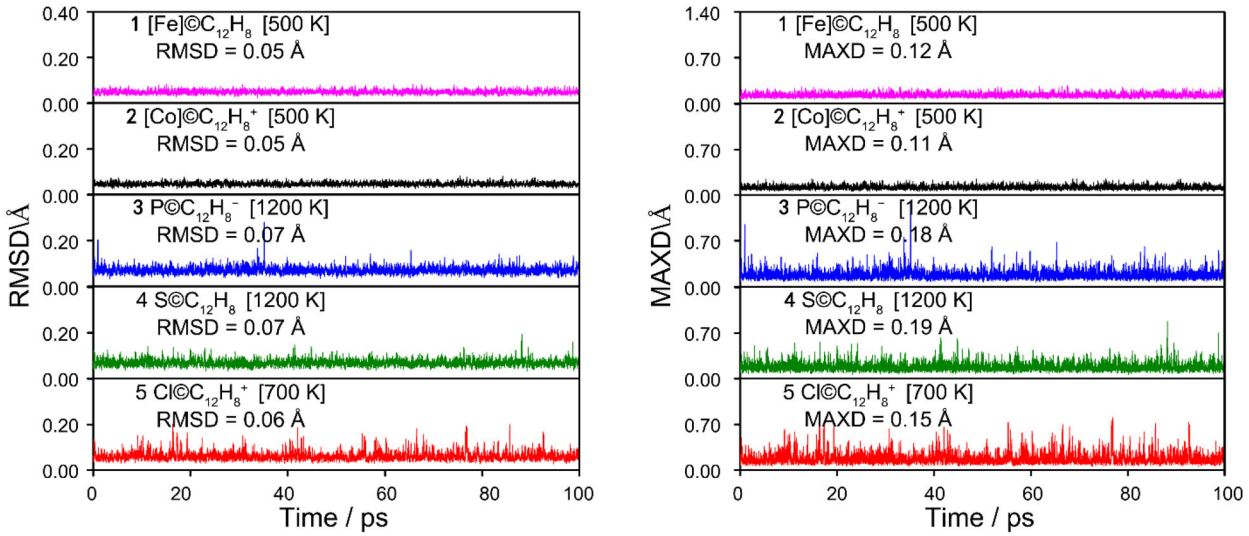

FIGURE 2 | BOMD simulations of $[Fe]C_{12}H_8$ (**1**) and $[Co]C_{12}H_8^+$ (**2**) at 500K, $PC_{12}H_8^-$ (**3**) and $SC_{12}H_8$ (**4**) at 1200 K, and $ClC_{12}H_8^+$ (**5**) at 700 K for 100 ps, with the corresponding average root-mean-square-deviation (RMSD) and maximum bond length deviation (MAXD) values indicated in Å.

also be designed.

$$12\ S©C_{12}H_8 \rightarrow (S©C_{12}H_4)_{12} + 24H_2 \quad (1)$$

It is also noticed that, with two extra-electrons attached to the triplet complexes, the D_{4h} $SC_{12}H_8$ (**4**) and D_{4h} $ClC_{12}H_8^+$ (**5**) are transformed into singlet D_{4h} $SC_{12}H_8^{2-}$ (**12**, $^1A_{1g}$) and D_{4h} $ClC_{12}H_8^-$ (**13**, $^1A_{1g}$), respectively, forming two perfect in-plane [5555] nonmetallo-annulene anions, as shown in Figure S2. The optimized $PC_{12}H_8^{3-}$ (**14**) turns out to have a slightly distorted C_{2v} geometry.

Additional theoretical calculations have also been performed on the perfect in-plane [5555] nonmetallo-annulene frameworks in D_{4h} $[P]C_{12}H_8^-$ (**15**, [P] = $P(CO)_2$) and D_{4h} $[As]C_{12}H_8^-$ (**16**, [As] = $As(CO)_2$) in Figure S3 and off-planed [5555] metallo-annulene frameworks in C_{4v} $[Ru]C_{12}H_8$ (**17**, [Ru] = $Ru(CO)_2$), C_{4v} $[Rh]C_{12}H_8^+$ (**18**, [Rh] = $Rh(CO)_2$), C_{4v} $[Os]C_{12}H_8$ (**19**, [Os] = $Os(CO)_2$), and C_{4v} $[Ir]C_{12}H_8^+$ (**20**, [Ir] = $Ir(CO)_2$) in Figure S4. The metal centers in **17**, **18**, **19**, and **20** are off-planed by 1.32 Å, 0.98 Å, 1.42 Å, and 1.16 Å, respectively, due to their relatively large atomic radii.

3.2 | Bonding Pattern and Aromaticity Analyses

Detailed AdNDP bonding pattern analyses help to comprehend the unique geometries and high stability of these novel [5555] annulene complexes. As clearly shown in Figure 3a, the singlet D_{4h} $[Fe]C_{12}H_8$ (**1,** [Fe] = $Fe(CO)_2$) possesses 8 2c-2e C-H σ bonds around the $[12]C_{12}H_8$ annulene with the occupation number of ON = 1.98 |e|, 12 2c-2e C-C σ bonds with ON = 1.98 |e| on the $[12]C_{12}H_8$ ligand, 1 1c-2e σ lone pair on the Fe center ($3d_{xy}$) with ON = 1.95 |e|, 2 1c-2e lone pairs on two O atoms on the two CO ligands with ON = 1.97, 2 2c-2e C-O σ bonds and 4 2c-2e C-O π bonds on the two CO ligands in axial direction with ON = 2.00 |e|, 2 2c-2e Fe-CO coordination σ-bonds with ON = 1.96 |e| in axial direction on the top and bottom, and 4 2c-2e Fe-C σ bonds with ON = 1.90 |e| between the η^4-Fe center and its four closest C neighbors on the inner-ring of the $C_{12}H_8$ annulene. The remaining seven delocalized π bonds include 2 5c-2e π bonds with ON = 1.82 |e| between the η^4-Fe center and its four closest C neighbors over the FeC_4 unit in which the Fe $3d_{xz}$ and $3d_{yz}$ atomic orbitals participate and 5 12c-2e π bonds over the $C_{12}H_8$ annulene plane with ON = 1.95-2.00 |e|. Such a bonding scheme indicates that the η^4-Fe center matches the 18-electron role. The overall seven delocalized π bonds over the perfect in-plane [5555] metallo-annulene framework matchthe [4n+2] Hückel's aromatic rule (n = 3) for a closed-shell π system, rendering overall π aromaticity to the system, similar to the situation in the experimentally observed D_{5h} $[Os]C_{15}H_{10}$ ([Os] = $Os(CO)_2$) (1) and theoretically proposed D_{5h} $MC_{15}H_{10}$ (M = Pt, Pd, Ni) [2]. As shown in Figure S5, detailed EDA-NOCV analyses indicate that there exist one effective σ-donation and two weak π-back-donations between the CO ligand and metal center in both D_{4h} $[Fe]C_{12}H_8$ (**1**) and D_{4h} $[Co]C_{12}H_8^+$ (**2**), indicating that the metal centers Fe and Co embedded in the planar annulene ligand sustain their σ-hole characteristics, similar to the situation in the previously reported planar- and bowl-shaped Metallo-phosphaporphyrins [53]. Figure S6a-e indicates that the 3D $[Co]C_{12}H_8^+$ (**2**), $[Ru]C_{12}H_8$ (**17**), $[Rh]C_{12}H_8^+$ (**18**), $[Os]C_{12}H_8$ (**19**), and $[Ir]C_{12}H_8^+$ (**20**) with an in-plane [5555] metallo-annulene framework all follow the same bonding pattern with $[Fe]C_{12}H_8$ (**1**).

The bonding pattern of the triplet D_{4h} $SC_{12}H_8$ (**4**) is comparatively depicted in Figure 3b. Such a perfect in-plane [5555] nonmetallo-annulene contains 8 2c-2e C-H σ bonds around the $C_{12}H_8$ annulene ligand with ON = 1.98 |e|, 12 2c-2e C-C σ bonds with ON = 1.98-1.99 |e| on the $C_{12}H_8$ annulene plane, 4 2c-2e S-C σ bonds with ON = 1.97 |e| between the η^4-S center and its four closest C neighbors on the inner ring, and 1 5c-2e π bond with ON = 2.00 |e| which the S $2p_z$ orbital participates in and renders local π-aromaticity to the S@C_4 structural unit at the center. The remaining 12 valence electrons are distributed in 5 doubly occupied 12c-2e π bonds with ON = 1.89–2.00 and 2 singly occupied 12c-1e π bonds delocalized over the $C_{12}H_8$ ligand, rendering overall π-aromaticity to the planar species matching Hückel's [4n] aromatic rule (n = 3) for an open-shell system. Such

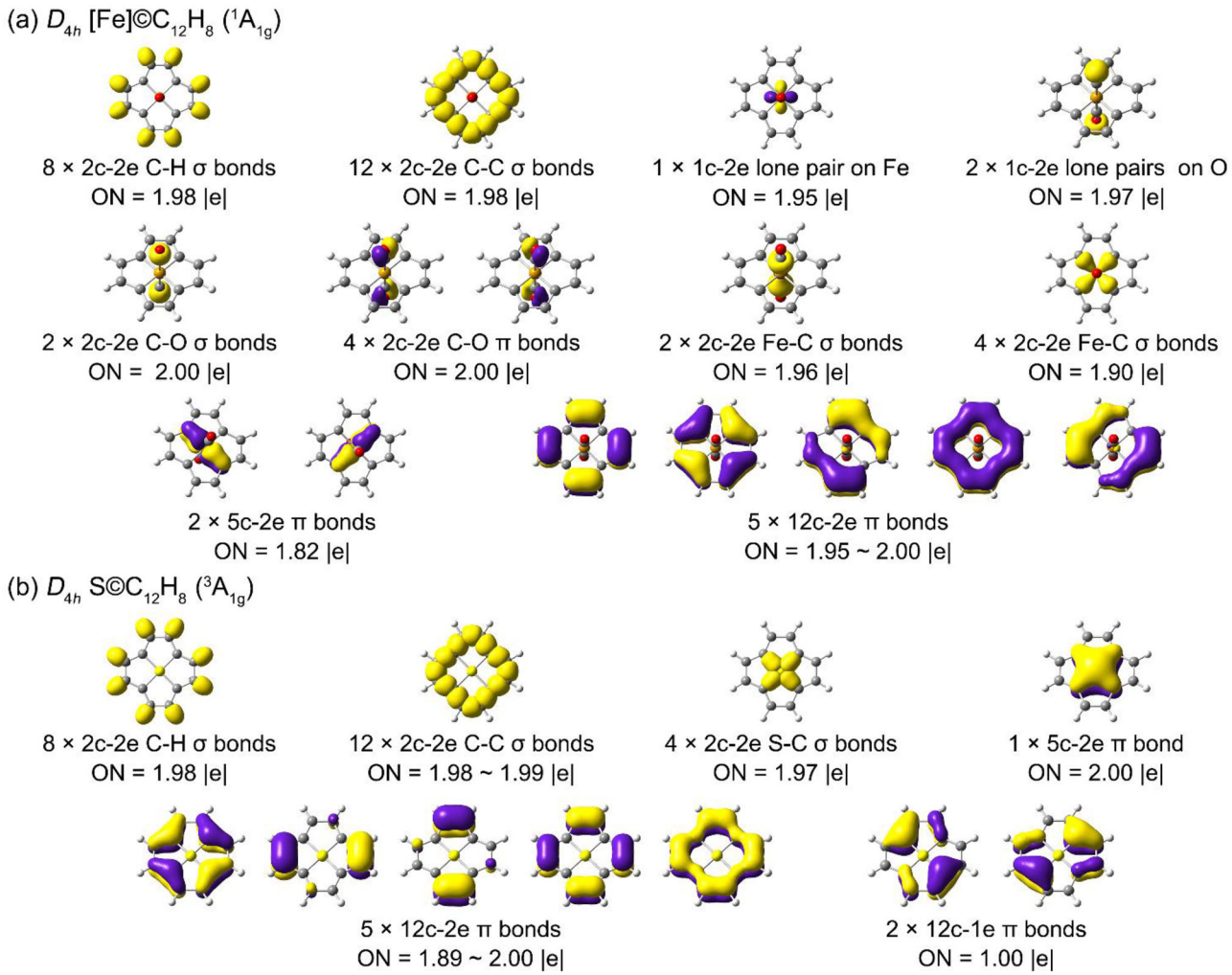

FIGURE 3 | AdNDP bonding patterns of (a) singlet D_{4h} [Fe]$C_{12}H_8$ (**1**, [Fe] = $Fe(CO)_2$) and (b) triplet D_{4h} $SC_{12}H_8$ (**4**), with the occupation numbers (ON) indicated.

a $4\sigma + 1\pi$ coordination bonding pattern between the η^4-S center and the [5555] annulene ligand effectively helps to maintain the perfect D_{4h} symmetry and high stability of the nonmetal-centered annulene complex. As shown in Figure S6f,g, the triplet D_{4h} $PC_{12}H_8^-$ (**3**) and D_{4h} $ClC_{12}H_8^+$ (**5**) exhibit the same bonding pattern as $SC_{12}H_8$ (**4**).

The ADNDP bonding patterns of C_{4v} [Fe]$C_{36}H_{16}$ (**6**), D_{4h} [Co]$C_{36}H_{16}^+$ (**7**), D_{4h} $PC_{36}H_{16}^-$ (**8**), D_{4h} $SC_{36}H_{16}$ (**9**), and C_s $ClC_{36}H_{16}^+$ (**10**) in Figure S7 strongly suggest that these 2D expanded [5555] annulene complexes all well retain the π-aromatic character of their parent structures. Similarly, the singlet D_{4h} $SC_{12}H_8^{2-}$ (**12**, $^1A_{1g}$), D_{4h} $ClC_{12}H_8^-$ (**13**, $^1A_{1g}$), D_{4h} [P]$C_{12}H_8^-$ (**15**, [P] = $P(CO)_2$) and D_{4h} [As]$C_{12}H_8^-$ (**16**, [As] = $As(CO)_2$) also prove to be π-aromatic in nature, as shown in their bonding patterns in Figure S8.

Detailed ICSS analyses help to further evaluate the aromatic characteristics of the most concerned complexes. Based on the calculated nucleus-independent chemical shift values in the vertical direction (NICS-ZZ), Figure 4a depicts the ICSS surfaces of D_{4h} [Fe]$C_{12}H_8$ (**1**), D_{4h} [Co]$C_{12}H_8^+$ (**2**), D_{4h} $PC_{12}H_8^-$ (**3**), D_{4h} $SC_{12}H_8$ (**4**) and D_{4h} $ClC_{12}H_8^+$ (**5**) with the Z-axis perpendicular to the [12]$C_{12}H_8$ annulene plane. Obviously, the spaces inside the $C_{12}H_8$ ring in the horizontal direction and within about 1.0 Å above the coordination centers in the vertical direction all belong to chemical shielding regions highlighted in yellow with negative NICS-ZZ values, while the chemical de-shielding areas highlighted in green with positive NICS values are located outside the [5555] $C_{12}H_8$ ring like a belt around the complex in the middle in the horizontal direction. The ICSSs of these [5555] metallo- and nonmetallo-annulene complexes all turn out to be similar to that of the experimentally observed D_{5h} [Os]$C_{15}H_{10}$ ([Os] = $Os(CO)_2$) (1) and theoretically proposed D_{5h} $MC_{15}H_{10}$ (M = Pt, Pd, Ni) (2), strongly evidencing their overall aromaticity in nature.

The visualized ACID and GIMIC plots in Figure 4b,c provide direct evidence to graphically display the ring currents induced by an external magnetic field in vertical directions perpendicular to the molecular planes. Both the ACID and GIMIC clockwise current density vectors indicated in Figure 4b,c for D_{4h} [Fe]$C_{12}H_8$ (**1**), D_{4h} [Co]$C_{12}H_8^+$ (**2**), D_{4h} $PC_{12}H_8^-$ (**3**), D_{4h} $SC_{12}H_8$ (**4**), and D_{4h} $ClC_{12}H_8^+$ (**5**) indicate that these [5555] metallo- and nonmetallo-annulene complexes are all aromatic in nature. These perfect planar aromatic complexes are expected to exhibit different magnetic behavior under the given orientation in relation to the external field, similar to the situation in benzene [54].

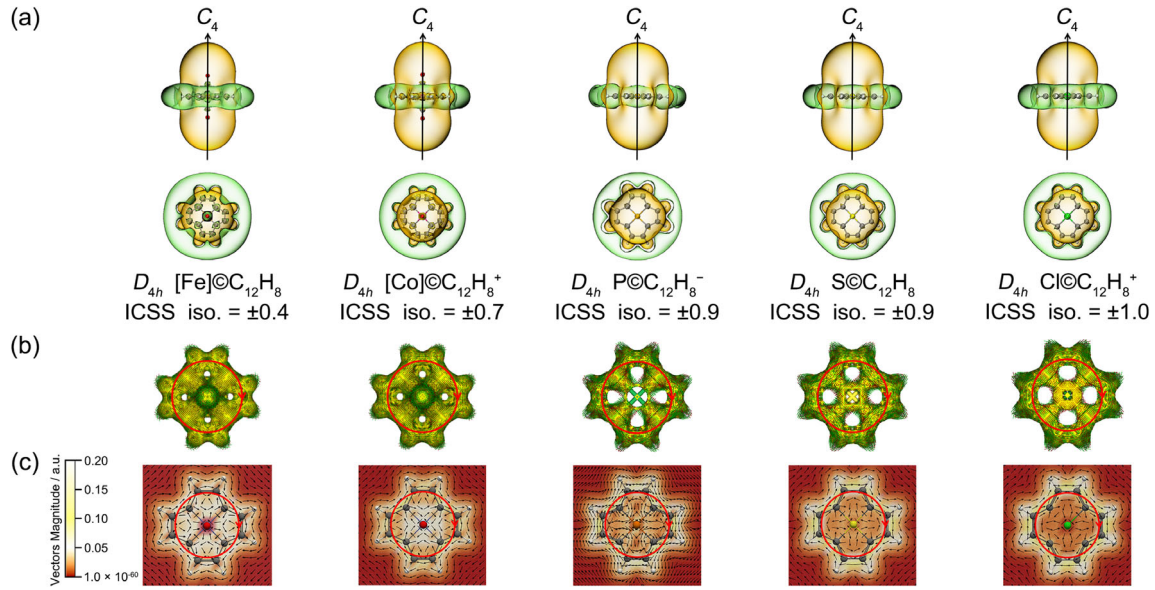

FIGURE 4 | (a) Calculated iso-chemical shielding surfaces (ICSSs) of D_{4h} [Fe]$C_{12}H_8$ (**1**), D_{4h} [Co]$C_{12}H_8^+$ (**2**), D_{4h} $PC_{12}H_8^-$ (**3**), D_{4h} $SC_{12}H_8$ (**4**), and D_{4h} $ClC_{12}H_8^+$ (**5**). Yellow and green regions stand for chemical shielding and de-shielding areas, respectively. (b) and (c) show their corresponding ACID and (c) GIMIC plots, respectively, with the color scales indicated in (c). The external magnetic field is perpendicular to the molecular plane. The red arrows represent directions of the ring currents at various positions on the ACID and GIMIC iso-surfaces.

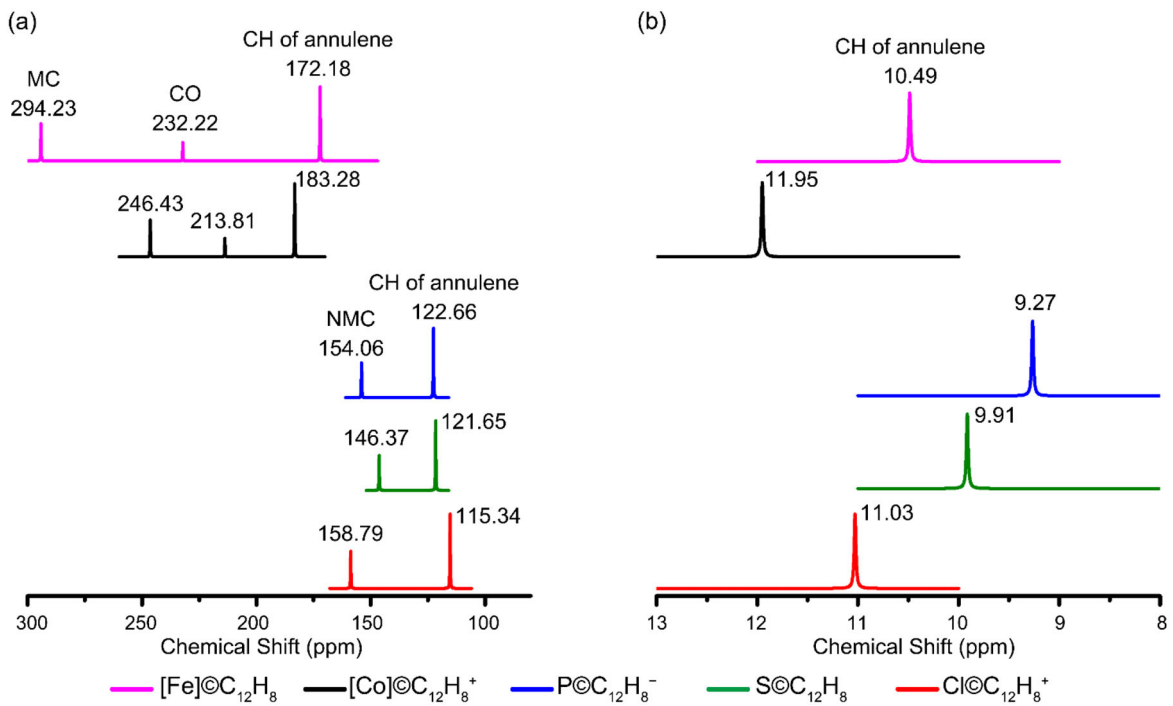

FIGURE 5 | Simulated (a) ^{13}C NMR and (b) ^{1}H NMR spectra of [Fe]$C_{12}H_8$ (1), [Co]$C_{12}H_8^+$ (2), $PC_{12}H_8^-$ (3), $SC_{12}H_8$ (4), and $ClC_{12}H_8^+$ (5), with the calculated chemical shift values indicated in ppm.

3.3 | Spectral Simulations

Figure 5 depicts the simulated ^{13}C and ^{1}H NMR spectra of D_{4h} [Fe]$C_{12}H_8$ (**1**), D_{4h} [Co]$C_{12}H_8^+$ (**2**), D_{4h} $PC_{12}H_8^-$ (**3**), D_{4h} $SC_{12}H_8$ (**4**), and D_{4h} $ClC_{12}H_8^+$ (**5**) to facilitate their future spectroscopic characterizations. As shown in the simulated ^{13}C NMR spectra in Figure 5a, D_{4h} [Fe]$C_{12}H_8$ (**1**) exhibits three characteristic chemical shifts at $\delta = 294.23$, 232.22, and 172.18 ppm corresponding to Fe*C*, *C*O, and *C*H of the system, respectively, while D_{4h} [Co]$C_{12}H_8^+$ (**2**) exhibits three peaks at δ = 246.43, 213.81, and 183.28 ppm which can be assigned to the Co*C*, *C*O, and *C*H of the species, respectively. Due to the absence of the two CO axial ligands in axial direction, D_{4h} $PC_{12}H_8^-$ (**3**), D_{4h} $SC_{12}H_8$ (**4**), and D_{4h} $ClC_{12}H_8^+$ (**5**) display only two ^{13}C NMR signals shifted to higher fields

at δ = 154.06/122.66, 146.37/121.65, and 158.79/115.34 ppm which correspond to the four C atoms bonded to nonmetal center and eight C atoms on the outer ring of the [5555] annulene ligand, respectively. The eight protons on the $C_{12}H_8$ annulene ligand in D_{4h} **1**, **2**, **3**, **4**, and **5** complexes are deshielded and chemically equivalent, resonating as singlet at δ = 10.49, 11.95, 9.27, 9.91, and 11.03 ppm in the corresponding ^{1}H NMR spectra of **1**, **2**, **3**, **4**, and **5** in Figure 5b, respectively, with the D_{4h} $[Co]C_{12}H_8^+$ (**2**) monocation possessing the largest calculated ^{1}H chemical shift. Detailed simulated IR, Raman, and UV-vis spectra of complexes **1–5** are collectively provided in Figure S9 to facilitate their experimental characterizations.

4 | Conclusions

Extensive first-principles theory investigations performed in this work present the viable possibility of a series of perfect in-plane [5555] metallo-annulene frameworks in 3D D_{4h} $[Fe]C_{12}H_8$ (**1**) and D_{4h} $[Co]C_{12}H_8^+$ (**2**) and perfect 2D in-plane [5555] nonmetallo-annulene complexes including D_{4h} $PC_{12}H_8^-$ (**3**), D_{4h} $SC_{12}H_8$ (**4**), and D_{4h} $ClC_{12}H_8^+$ (**5**), with $[12]C_{12}H_8$ as the universal ligand. In these highly stable metal-/nonmetal-centered annulene complexes, both the ptM and ptNM centers and the $[12]C_{12}H_8$ annulene ligand match geometrically and electronically, forming effective coordination bonding patterns to help stabilize the systems. The ptM $3d_{xz}$ and $3d_{yz}$ and ptNM $2p_z$ orbitals participate in the delocalized π-bonding systems of the complexes and contribute to the overall π-aromaticity of the concerned species, in strong contrast to the out-of-plane π-coordination bonding pattern in traditional metallo-annulene complexes. These complexes can be extended in 2D to form the planar or quasi-planar **6–10** and in 3D to generate the tubular nanobelt **11** via partial dehydrogenations. Syntheses and characterization of such [5555] metallo- and nonmetallo-annulene complexes and their corresponding 1D, 2D, and 3D nanocrystals using the right precursors under suitable conditions in future experiments would effectively enrich the chemistry and materials science of annulene complexes.

Acknowledgments

This work was supported by the National Natural Science Foundation of China (22373061 and 92461303 to S. D. L).

Conflicts of Interest

The authors declare no conflicts of interest.

References

1. B. B. Xu, D. F. Chen, K. D. Ruan, et al., "Metal-Centred Planar [15]Annulenes," *Nature* 641 (2025): 106–111.

2. X. N. Zhao, J. F. Wei, Q. Chen, and S. D. Li, "Prediction of Perfect Aromatic In-Plane [55555] Metallo-Annulenes," *European Journal of Inorganic Chemistry* 28 (2025): e202500420.

3. E. L. Spitler, C. A. Johnson, and M. M. Haley, "Renaissance of Annulene Chemistry," *Chemical Reviews* 106 (2006): 5344–5386.

4. F. Sondheimer and R. Wolovsky, "Unsaturated Macrocyclic Compounds. XXI.1The Synthesis of a Series of Fully Conjugated Macrocyclic Polyene-polyynes (Dehydro-annulenes) From 1,5-Hexadiyne," *Journal of the American Chemical Society* 84 (1962): 260–269.

5. T. J. Kealy and P. L. Pauson, "A New Type of Organo-Iron Compound," *Nature* 168 (1951): 1039–1040.

6. D. Astruc, "The Numerous Paths Of Ferrocene," *Nature Chemistry* 15 (2023): 1650.

7. D. Seyferth, "Bis(benzene)chromium. 2. Its Discovery by E. O. Fischer and W. Hafner and Subsequent Work by the Research Groups of E. O. Fischer, H. H. Zeiss, F. Hein, C. Elschenbroich, and Others," *Organometallics* 21 (2002): 2800–2820.

8. G. Pampaloni, "Aromatic Hydrocarbons as Ligands. Recent Advances In The Synthesis, The Reactivity And The Applications Of Bis(H6-Arene) Complexes," *Coordination Chemistry Reviews* 254 (2010): 402–419.

9. A. Streitwieser Jr. and U. Mueller-Westerhoff, "Bis(cyclooctatetraenyl) Uranium (uranocene). A New Class Of Sandwich Complexes That Utilize Atomic F Orbitals," *Journal of the American Chemical Society* 90 (1968): 7364.

10. S. Arndt and J. Okuda, "Mono(cyclopentadienyl) Complexes of the Rare-Earth Metals," *Chemical Reviews* 102 (2002): 1953–1976.

11. M. N. Bochkarev, "Synthesis, Arrangement, and Reactivity of Arene−Lanthanide Compounds," *Chemical Reviews* 102 (2002): 2089–2118.

12. L. Münzfeld, S. Gillhuber, A. Hauser, et al., "Synthesis And Properties Of Cyclic Sandwich Compounds," *Nature* 620 (2023): 92–96.

13. Z. Zhou and M. A. Petrukhina, "Adding Multiple Electrons to Helicenes: How they respond?" *Chemical Science* 16 (2025): 468–479.

14. S. Krieck, H. Görls, L. Yu, M. Reiher, and M. Westerhausen, "Stable "Inverse" Sandwich Complex With Unprecedented Organocalcium(I): Crystal Structures of [(thf) 2 Mg(Br)-C 6 H 2 -2,4,6-Ph 3] and [(thf) 3 Ca{μ-C 6 H 3 -1,3,5-Ph 3 }Ca(thf) 3]," *Journal of the American Chemical Society* 131 (2009): 2977–2985.

15. T. D. Lash, "Carbaporphyrinoid Systems," *Chemical Reviews* 117 (2017): 2313–2446.

16. M. S. Thakur, N. Singh, A. Sharma, et al., "Metal-Coordinated Macrocyclic Complexes In Different Chemical Transformations," *Coordination Chemistry Reviews* 471 (2022): 214739.

17. M. J. Białek, K. Hurej, H. Furuta, and L. Latos-Grażyński, "Organometallic Chemistry Confined Within A Porphyrin-Like Framework," *Chemical Society Reviews* 52 (2023): 2082–2144.

18. V. Grover and M. Ravikanth, "Coordination Chemistry Of Porphycenes," *Coordination Chemistry Reviews* 516 (2024): 215999.

19. C. Q. Zhu and H. P. Xia, "Carbolong Chemistry: A Story of Carbon Chain Ligands and Transition Metals," *Accounts of Chemical Research* 51 (2018): 1691–1700.

20. D. F. Chen, Y. H. Hua, and H. P. Xia, "Metallaaromatic Chemistry: History and Development," *Chemical Reviews* 120 (2020): 12994–13086.

21. Q. Su, J. P. Ding, Z. H. Du, et al., "Recent Advances in the Reactions of Cyclic Carbynes," *Molecules* 25 (2020): 5050.

22. M. Luo, D. F. Chen, Q. Li, and H. P. Xia, "Unique Properties and Emerging Applications of Carbolong Metallaaromatics," *Accounts of Chemical Research* 56 (2023): 924–937.

23. M. J. Frisch, G. W. Trucks, H. B. Schlegel, et al., "Gaussian 16, Revision C.01, Gaussian, Inc., Wallingford, CT, USA," (2016).

24. C. Adamo and V. Barone, "Toward Reliable Density Functional Methods Without Adjustable Parameters: The PBE0 Model," *The Journal of Chemical Physics* 110 (1999): 6158–6170.

25. P. J. Stephens, F. J. Devlin, C. F. Chabalowski, and M. J. Frisch, "Ab Initio Calculation of Vibrational Absorption and Circular Dichroism Spectra Using Density Functional Force Fields," *The Journal of Physical Chemistry* 98 (1994): 11623–11627.

26. M. S. Gordon, J. S. Binkley, J. A. Pople, W. J. Pietro, and W. J. Hehre, "Self-Consistent Molecular-Orbital Methods. 22. Small Split-Valence Basis Sets For Second-Row Elements," *Journal of the American Chemical Society* 104 (1982): 2797–2803.

27. W. J. Pietro, M. M. Francl, W. J. Hehre, D. J. DeFrees, J. A. Pople, and J. S. Binkley, "Self-Consistent Molecular Orbital Methods. 24. Supplemented Small Split-Valence Basis Sets For Second-Row Elements," *Journal of the American Chemical Society* 104 (1982): 5039–5048.

28. T. Clark, J. Chandrasekhar, G. W. Spitznagel, and P. V. R. Schleyer, "Efficient Diffuse Function-Augmented Basis Sets For Anion Calculations. III. The 3-21+G Basis Set For First-Row Elements, Li–F," *Journal of Computational Chemistry* 4 (1983): 294–301.

29. D. Andrae, U. Häußermann, M. Dolg, H. Stoll, and H. Preuß, "Energy-Adjustedab Initio Pseudopotentials For The Second And Third Row Transition Elements," *Theoretica Chimica Acta* 77 (1990): 123–141.

30. D. Y. Zubarev and A. I. Boldyrev, "Developing Paradigms Of Chemical Bonding: Adaptive Natural Density Partitioning," *Physical Chemistry Chemical Physics* 10 (2008): 5207.

31. T. Lu and F. W. Chen, "Multiwfn: A Multifunctional Wavefunction Analyzer," *Journal of Computational Chemistry* 33 (2012): 580–592.

32. T. Lu, "A Comprehensive Electron Wavefunction Analysis Toolbox For Chemists, Multiwfn," *The Journal of Chemical Physics* 161 (2024): 082503.

33. J. VandeVondele, M. Krack, F. Mohamed, M. Parrinello, T. Chassaing, and J. Hutter, "Quickstep: Fast And Accurate Density Functional Calculations Using A Mixed Gaussian And Plane Waves Approach," *Computer Physics Communications* 167 (2005): 103–128.

34. T. D. Kühne, M. Iannuzzi, M. Del Ben, et al., *Journal of Chemical Physics* 152 (2020): 194103.

35. J. M. Millam, V. R. Bakken, W. Chen, W. L. Hase, and H. B. Schlegel, "Ab Initio Classical Trajectories On The Born–Oppenheimer Surface: Hessian-Based Integrators Using Fifth-Order Polynomial And Rational Function Fits," *The Journal of Chemical Physics* 111 (1999): 3800–3805.

36. S. Klod and E. Kleinpeter, *Journal of the Chemical Society, Perkin Transactions 2* (2001): 1893.

37. Y. S. Liu, B. Quan, X. H. Liang, et al., "Energetic Metal-Organic Frameworks Deflagration Enabled Ultrafast Low-Temperature Synthesis Of Ultra-Light Magnetic Nanoparticles Decorated High-Lossy Materials," *Carbon* 165 (2020): 286–295.

38. D. Geuenich, K. Hess, F. Köhler, and R. Herges, "Anisotropy of the Induced Current Density (ACID), a General Method to Quantify and Visualize Electronic Delocalization," *Chemical Reviews* 105 (2005): 3758–3772.

39. R. Herges and D. Geuenich, "Delocalization of Electrons in Molecules," *The Journal of Physical Chemistry A* 105 (2001): 3214–3220.

40. H. Fliegl, S. Taubert, O. Lehtonen, and D. Sundholm, "The Gauge Including Magnetically Induced Current Method," *Physical Chemistry Chemical Physics* 13 (2011): 20500.

41. D. Sundholm, H. Fliegl, and R. J. F. Berger, "Calculations Of Magnetically Induced Current Densities: Theory And Applications," *WIREs Computational Molecular Science* 6 (2016): 639–678.

42. J. Jusélius, D. Sundholm, and J. Gauss, *Journal of Chemical Physics* 121 (2004): 3952.

43. W. Humphrey, A. Dalke, and K. Schulten, "VMD: Visual Molecular Dynamics," *Journal of Molecular Graphics* 14 (1996): 33–38.

44. L. Persistence of Vision Raytracer Pty, POV-Ray 3.7, http://www.povray.org (accessed on Nov 20, 2019).

45. A. H. Squillacote, J. Ahrens, C. Law, B. Geveci, K. Moreland, and B. King, *The paraview guide* (2007).

46. U. Ayachit, *The Paraview Guide: A Parallel Visualization Application* (Kitware, Inc., 2015).

47. A. V. Marenich, C. J. Cramer, and D. G. Truhlar, "Universal Solvation Model Based on Solute Electron Density and on a Continuum Model of the Solvent Defined by the Bulk Dielectric Constant and Atomic Surface Tensions," *The Journal of Physical Chemistry B* 113 (2009): 6378–6396.

48. T. Ziegler and A. Rauk, "On the calculation of bonding energies by the Hartree-Fock Slater method," *Theoretica Chimica Acta* 46 (1977): 1–10.

49. M. P. Mitoraj, A. Michalak, and T. Ziegler, "A Combined Charge and Energy Decomposition Scheme for Bond Analysis," *Journal of Chemical Theory and Computation* 5 (2009): 962–975.

50. M. Mitoraj and A. Michalak, "Donor–Acceptor Properties of Ligands From the Natural Orbitals for Chemical Valence," *Organometallics* 26 (2007): 6576–6580.

51. G. Te Velde, F. M. Bickelhaupt, E. J. Baerends, et al., "Chemistry With ADF," *Journal of Computational Chemistry* 22 (2001): 931–967.

52. A. Rodríguez-Rubio, H. Zhu, K. Man Cheung, et al., "Synthesis Of Triple-Stranded Porphyrin Nanobelts," *Science* 390 (2025): 290–293.

53. M. Paco-Chipana, A. E. Kuznetsov, and A. Muñoz-Castro, "Evaluation of Planar- and Bowl-Shaped Metallophosphaporphyrins. Inclusion of Steric Effects in P4-Metalloporphyrins Counterparts," *Advanced Theory and Simulations* 9 (2026): e02185.

54. A. G. Papadopoulos, N. D. Charistos, and A. Muñoz-Castro, "Magnetic Response of Aromatic Rings Under Rotation: Aromatic Shielding Cone of Benzene Upon Different Orientations of the Magnetic Field," *Chemphyschem* 18 (2017): 1499–1502.

Supporting Information

Additional supporting information can be found online in the Supporting Information section.

Supporting File: chem71322-sup-0001-SuppMat.pdf